

# 1 Fast and accurate imputation of genotypes 2 from noisy low-coverage sequencing data 3 in bi-parental populations

4 Cécile Triay<sup>1,§</sup> & Alice Boizet<sup>2,§</sup>, Christopher Fragoso<sup>3,4</sup>, Anestis Gkanogiannis<sup>5</sup>,  
5 Jean-François Rami<sup>2</sup>, Mathias Lorieux<sup>1,5,\*</sup>

6 <sup>1</sup>DIADÉ, University of Montpellier, IRD, Cirad, Montpellier, France

7 <sup>2</sup>AGAP, University of Montpellier, Cirad, INRAE, Montpellier SupAgro, Montpellier, France

8 <sup>3</sup>Verinomics, Inc., 5 Science Park, New Haven, CT 06511, USA

9 <sup>4</sup>Department of Molecular, Cellular, and Developmental Biology, Yale University, New Haven, Connecticut 06511

10 <sup>5</sup>Agrobiotechnology Unit, Alliance Bioversity-CIAT, International Center for Tropical Agriculture, Cali, Colombia.

11 \*Corresponding author

12 <sup>§</sup>Equivalent contribution

## 13 Abstract

14 **Motivation:** Genotyping of bi-parental populations can be performed with low-coverage next-generation  
15 sequencing (LC-NGS). This allows the creation of highly saturated genetic maps at reasonable cost, precisely  
16 localized recombination breakpoints (i.e., the crossovers), and minimized mapping intervals for  
17 quantitative-trait locus analysis.

18 The main issues with these low-coverage genotyping methods are (1) poor performance at heterozygous loci,  
19 (2) high percentage of missing data, (3) local errors due to erroneous mapping of sequencing reads and  
20 reference genome mistakes, and (4) global, technical errors inherent to NGS itself.

21 Recent methods like Tassel-FSFHap or LB-Impute are excellent at addressing issues 1 and 2, but nonetheless  
22 perform poorly when issues 3 and 4 are persistent in a dataset (i.e., “noisy” data). Here, we present a new  
23 algorithm for imputation of LC-NGS data that eliminates the need of complex pre-filtering of noisy data,  
24 accurately types heterozygous chromosomal regions, precisely estimates crossover positions, corrects  
25 erroneous data, and imputes missing data. The imputation of genotypes and recombination breakpoints is  
26 based on maximum-likelihood estimation. We compare its performance with Tassel-FSFHap and LB-Impute  
27 using simulated data and two real datasets. Furthermore, the algorithm is much faster than Hidden Markov  
28 Model methods.

29 **Availability:** NOISYmputer and its source code are available as a multiplatform (Linux, macOS, Windows) Java  
30 executable at the URL

31 [https://gitlab.cirad.fr/noisympouter/noisympouterstandalone/-/tree/1.0.0-RELEASE?ref\\_type=tags](https://gitlab.cirad.fr/noisympouter/noisympouterstandalone/-/tree/1.0.0-RELEASE?ref_type=tags).

## 32 Introduction

33 In genetic studies, bi-parental genetic populations can be created from inbred parental lines using various  
34 crossing systems, e.g., F<sub>2</sub> intercross issued from F<sub>1</sub> self-pollination (F<sub>2</sub>) and recombinant inbred lines by single  
35 seed descent (SSD). These populations are used to create recombination maps and, if phenotypes are  
36 available, to find gene or quantitative-trait locus (QTL) genomic positions.

37 To do so, each individual of the population under study has to be characterized for its genomic content – or  
38 “genotyped” at many loci. This can be done using different molecular biology techniques, including various  
39 types of molecular markers. The gold standard for genetic variant discovery is obtained by different  
40 next-generation sequencing (NGS) techniques like restriction site-associated DNA sequencing (RADseq)  
41 (Davey and Blaxter 2010), genotyping by sequencing (GBS) (Elshire *et al.* 2011), and whole-genome  
42 sequencing (WGS) (Huang *et al.* 2009). These techniques provide very large numbers of markers and  
43 therefore facilitate the construction of highly saturated genetic maps. This provides accurate locations of  
44 recombination breakpoints in each individual, which is important for a number of applications, e.g., studies of

45 local recombination rate, genetic maps comparison, or QTL detection. Though NGS is less and less expensive to  
46 implement, sequencing a large number of samples can still be costly, and is commonly applied via reduced  
47 representation (RRS-NGS) or low-coverage (LC-NGS) strategies to reduce genotyping costs.

48 Reducing sequencing costs through minimized per-sample coverage has an important experimental downside:  
49 LC-NGS mechanically introduces a series of issues, the main ones being:

50 - **Issue 1: Low power to detect heterozygosity under low coverage:** For example, if only one sequencing  
51 read is generated at a locus, only one of the two alleles is revealed. As each additional read has a 0.5  
52 probability of detecting the second allele, even 3 reads have only 0.75 probability of detecting a  
53 heterozygous call. Spread over thousands of sites, extensive inaccuracy in heterozygous regions becomes  
54 highly problematic.

55 - **Issue 2: Extensive genotype missingness:** The sparse distribution of reads at low coverage (3X coverage,  
56 for example, only implies an *average* of 3 reads per site) results in a complete lack of reads at some  
57 variant loci. Even in plants, which contain more genetic variation than humans, there are 6-22 SNPs per  
58 1 Kb, resulting in abundant opportunity for non-reference variant missingness under low coverage (Xu *et*  
59 *al.* 2017).

60 - **Issue 3: Errors due to erroneous mapping of sequencing reads:** NGS technologies are based on short  
61 reads (e.g., 150 base pair, paired-end Illumina technology). Due to the combinatorial limitation of the  
62 sequence contained in short reads, multiple mapping locations may be identified, especially in plant  
63 genomes which exhibit much more repetitive content than human genomes. Additionally, in plants, such  
64 as rice, structural variation specific to subpopulations may be completely missing in single reference  
65 genomes. These assembly errors, omissions, and challenges posed by repetitious regions are sources of  
66 erroneous variants. Moreover, outright assembly errors may cause consistent, yet locally encountered  
67 genotyping errors.

68 - **Issue 4: Technical errors inherent to NGS methodology:** Sequencing errors may be globally introduced at  
69 a variety of stages in the NGS pipeline, from errors incurred in PCR-dependent library construction to  
70 NGS sequencing itself. The initial GBS protocol is known to generate libraries contaminated by chimeric  
71 inserts (Heffelfinger *et al.* 2014). Although rare, these errors may become problematic at low coverage, as  
72 additional reads refuting an erroneous call may not be available at a given locus.

73 Common imputation algorithms implemented in computer programs like Beagle (Browning and Browning  
74 2007; Browning *et al.* 2021) or Impute2 (Howie *et al.* 2012), although very accurate in diversity panels, are  
75 not well adapted to the bi-parental context since they rely on large databases to infer haplotypes. Efficient  
76 methods have been recently developed to impute genotypic data derived from LC-NGS assays in bi-parental  
77 populations. For instance, Tassel-FSFHap (thereafter simply FSFHap) (Swarts *et al.* 2014) and LB-Impute  
78 (Fragoso *et al.* 2016) can all address issues 1 and 2 accurately. Yet, these methods can produce inaccurate  
79 results when the errors mentioned in issues 3 and 4 – thereafter called “noisy data” – are too frequent. Thus,  
80 these methods might require additional bioinformatic steps to filter out low-quality markers before and after  
81 imputation. Even then, troublesome markers might not be detected easily and could alter dramatically the  
82 quality of the imputation and the final genetic map.

83 In this work, we present NOISYmputer, a maximum likelihood estimation algorithm for imputation of LC-NGS  
84 data that eliminates the need of complex pre-filtering of noisy data, accurately finds heterozygous  
85 chromosomal regions, corrects erroneous data, imputes missing data and precisely locates the recombination  
86 breakpoints (i.e., the meiotic crossovers). We test its accuracy using simulated data and we compare its  
87 performance with FSFHap, LB-Impute using three datasets: (1) a rice F<sub>2</sub> population sequenced by WGS, (2) a  
88 maize F<sub>2</sub> population sequenced by GBS and (3) 84 simulated F<sub>2</sub> populations with controlled depth, error rate  
89 and marker density. The algorithm is implemented in NOISYmputer, a multiplatform Java command line  
90 program (see “Availability” section).

## 91 Design and implementation

### 92 Imputation method

93 In this section we describe the main imputation algorithm, which is applied separately to each chromosome.  
94 The imputation can be preceded or followed by different filtering options in NOISYmputer (details in next  
95 section) that can be applied to reduce or eliminate the noise in the data (Figure 1).

96 By imputation, we mean here guessing, confirming or correcting the genotype at a SNP site in a sample.  
97 LC-NGS generates poor information in heterozygous regions (see explanation on the confounding effect in  
98 SNPs with one or few reads – issue 1 of the Introduction section). Conversely, homozygous regions are much  
99 less prone to these confounding effects. Yet, missing data (issue 2), noisiness (issue 3) and sequencing errors  
100 (issue 4) can lower the power to identify homozygous diplotypes (*i.e.*, the combination of two gametic  
101 haplotypes). The general idea of the algorithm is, like in Hidden Markov Model (HMM), to use information of  
102 various SNPs around the imputed SNP, leaving unimputed the regions surrounding the recombination  
103 breakpoints laying between the two diplotypes. The locations of the recombination breakpoints are then  
104 inferred. Furthermore, instead of modeling error rates, we take an iterative approach to estimate them (Figure  
105 1).

#### 106 Imputation - Step 1: Genotype calling

107 Let's consider a chromosome of an  $F_2$  individual with one single recombination breakpoint that separates a  
108 homozygous diplotype (AA; BB) from a heterozygous diplotype (AB, or BA, equivalent thereafter). Let's also  
109 consider a set of SNPs evenly dispersed on the physical genome, say, every 500 base pairs (bp). In the AA  
110 diplotype, and far from the breakpoint location, all SNPs should be genotyped as AA, except from the different  
111 kinds of errors cited above. To determine the genotype of a particular SNP, and due to these errors, one must  
112 consider not only its score in the VCF, but also its immediate "environment", that is, the SNPs that are located  
113 just before and just after it along the chromosome. Those surrounding SNPs help identify a potential error in  
114 the SNP scoring. Different approaches can be taken to look at the SNP environment. In segregating  
115 populations, the vast majority of the genome is exempt from crossing overs. Indeed, when implementing a  
116 sliding window method like described hereby, the expected proportion of the genome with no recombination  
117 in the window is  $P_{noXO} \approx 1 - \left(\frac{1}{100N}\right)D(8m - 2)$ , where  $m$  is the number of SNPs in the sliding window,  $N$  is  
118 the total number of SNPs, and  $D$  is the expected genome size in centimorgans (cM). Hence, in almost the entire  
119 genome except the breakpoint regions there are only two or three possible diplotypes, depending on the  
120 population type. Thus, instead of calculating all the likelihoods of possible paths (like in Hidden Markov Model  
121 methods), the problem is reduced to calculate the likelihoods of the data for the three possible diplotypes.  
122 Furthermore, there is no need to include transition (*i.e.*, recombination) probabilities. The main advantage of  
123 this approach is its computation time, which increases linearly according to the diplotype size, while the time  
124 complexity is  $O(T \times S^2)$  for the Viterbi algorithm applied to resolve fully connected Hidden Markov Model  
125 processes, with  $T$  being the length of the sequence of observations and  $S$  being the number of hidden states.  
126 We now describe the algorithm with the example of an  $F_2$  population.

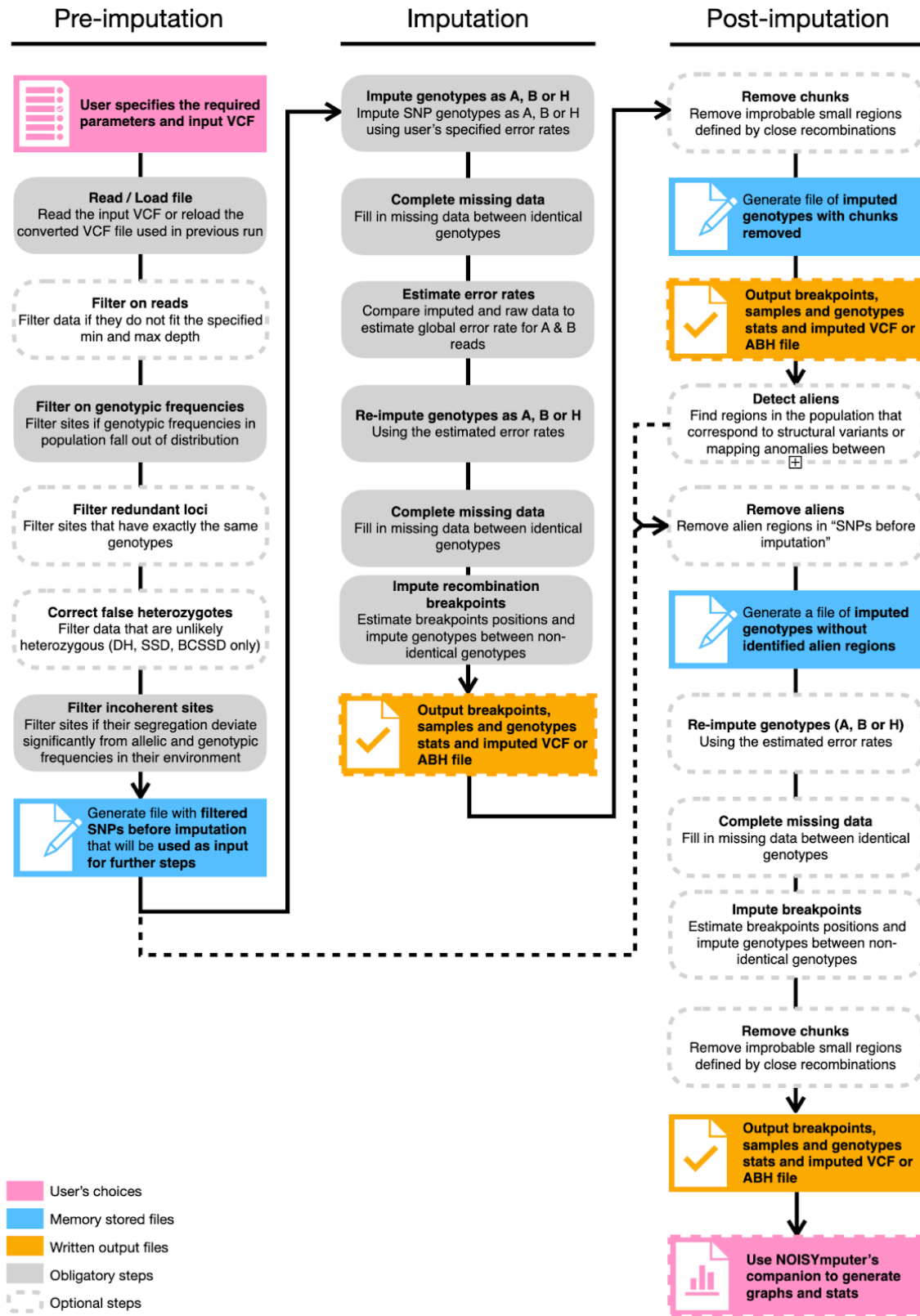
127 In practice, one defines starting values for error rates for reads A ( $e_A$ ) and B ( $e_B$ ), being respectively the  
128 probability of observing a B read ( $O_B$ ) whereas the genotype is truly AA and observing an A read ( $O_A$ ) whereas  
129 the genotype is truly a BB

$$130 \quad e_A = p(O_B|AA) \quad e_B = p(O_A|BB)$$

131 We allow different error rates for A and B reads since the A and B parents are generally not equally  
132 (genetically) distant from the reference genome. For example, once could set  $e_A = 0.005$  and  $e_B = 0.003$  if  
133 Parent B is closer genetically to the Reference genome than Parent A is. Those values will be automatically  
134 refined after one or several rounds of imputation.

135 Thus, at homozygous sites, the probability of observing an A read if the true genotype is AA is

$$136 \quad p(O_A|AA) = 1 - e_A$$



137

138 **Figure 1.** NOISYmputer's workflow. It is composed of three major phases: pre-imputation, imputation and post-imputation. Some  
 139 steps are optional (dashed borders) while others are required for the algorithm to complete.

140 and the probability of observing a B read if the true genotype is BB is

$$141 \quad p(O_B|BB) = 1 - e_B$$

142 At heterozygous (AB) sites, and assuming that the A and B reads have the same chance to occur, the  
143 probabilities of observing A and B reads are

$$144 \quad p(O_A|AB) = \frac{1}{2} p(O_A|AA) + \frac{1}{2} p(O_A|BB) = \frac{1}{2} (1 - e_A) + \frac{1}{2} e_B$$

$$145 \quad p(O_B|AB) = \frac{1}{2} p(O_B|BB) + \frac{1}{2} p(O_B|AA) = \frac{1}{2} (1 - e_B) + \frac{1}{2} e_A$$

146 Let's consider a chromosome with  $n$  SNPs. For each site  $SNP_j$  of the chromosome, we define a symmetrical  
147 window ( $W_j$ ) containing the  $SNP_j$  at its center,  $m$  SNPs before it in the sequence and  $m$  SNPs after it (with read  
148 count  $> 0$ ). SNPs that are located in chromosome ends are omitted, since it is not possible to define  
149 symmetrical windows around them. This case is discussed later on.

150 For each site  $SNP_i$  of the  $W_j$  window three situations are possible: i) the genotype  $G_i$  of the  $SNP_i$  is AA  
151 (homozygous for parent A allele), ii) the genotype  $G_i$  is BB (homozygous for parent B allele) or iii) the  
152 genotype  $G_i$  is AB (heterozygous).

153 By using the binomial distribution with sample size equal to  $n_i$  and the number of successes equal to  $nA_i$  (and  
154 thus of fails equal to  $nB_i$ ), we estimate the likelihood of observing a given combination of reads ( $nA_i$  and  $nB_i$   
155 as  $n_i = nA_i + nB_i$ ) at  $SNP_i$ , knowing already the probability of observing A reads under the three possible  
156 genotypes:

$$157 \quad P[nA_i | p(O_A | AA)] = \binom{n_i}{nA_i} p(O_A | AA)^{nA_i} (1 - p(O_A | AA))^{n_i - nA_i} = \binom{n_i}{nA_i} p(O_A | AA)^{nA_i} p(O_B | AA)^{nB_i}$$

$$158 \quad P[nA_i | p(O_A | BB)] = \binom{n_i}{nA_i} p(O_A | BB)^{nA_i} (1 - p(O_A | BB))^{n_i - nA_i} = \binom{n_i}{nA_i} p(O_A | BB)^{nA_i} p(O_B | BB)^{nB_i}$$

$$159 \quad P[nA_i | p(O_A | AB)] = \binom{n_i}{nA_i} p(O_A | AB)^{nA_i} (1 - p(O_A | AB))^{n_i - nA_i} = \binom{n_i}{nA_i} p(O_A | AB)^{nA_i} p(O_B | AB)^{nB_i}$$

160 Since the binomial factor is the same for the three possible genotypes, it can be omitted in the calculations.  
161 Then, individual relative probabilities that the genotype  $G_i$  of the  $SNP_i$  is AA, BB or AB are defined as:

$$162 \quad p(G_i = X) = P[nA_i | p(O_A | X)] / \sum_X P[nA_i | p(O_A | X)], \text{ with } X = AA, BB, AB$$

163 The probabilities for the window's diplotype around the  $SNP_j$  to be AA, BB or AB are obtained by multiplying  
164 the individual probabilities of all the SNPs in the window. As multiplication of probabilities can result in very  
165 small numbers, we add their logarithms instead to avoid reaching the precision limit of the computer:

$$166 \quad \rho_X = \sum_{i=SNP_j-m}^{SNP_j+m} \log[p(G_i = X)], \text{ with } X = AA, BB, AB$$

167 Finally, the relative probabilities for the window's  $W_j$  around the  $SNP_j$  to be AA, BB or AB are defined as:

$$168 \quad P(W_j = AA) = \exp(\rho_{AA}) / (\exp(\rho_{AA}) + \exp(\rho_{BB}) + \exp(\rho_{AB}))$$

$$169 \quad P(W_j = BB) = \exp(\rho_{BB}) / (\exp(\rho_{AA}) + \exp(\rho_{BB}) + \exp(\rho_{AB}))$$

170 
$$P(W_j = AB) = \exp(\rho_{AB}) / (\exp(\rho_{AA}) + \exp(\rho_{BB}) + \exp(\rho_{AB}))$$

171 A genotype is assigned to the SNP  $j$  if the relative probability of its surrounding window is superior to a given  
 172 threshold  $\alpha$ . To guarantee that no SNP is falsely genotyped, the  $\alpha$  threshold is set to a very stringent value  
 173 (0.999 by default). SNPs with  $P(W_j) < \alpha$  for all genotypes are assigned a missing data value.

174 We repeat the process for each SNP  $j$  of the chromosome. For chromosome ends, the procedure is similar  
 175 except that the half-window on the end side is smaller due to the lack of sites available to the left or right of  
 176  $SNP_j$ .

177 This leaves two types of chromosomal regions unimputed and filled with missing data: 1) regions between  
 178 imputed chromosome segments with identical diplotypes and for which none of the criteria are matched to  
 179 assign a genotype, and 2) regions near recombination breakpoints.

### 180 Imputation - Step 2: Gap filling and error rate estimation

181 Step 2 consists in (i) filling the unimputed regions with the surrounding genotype, with the condition that they  
 182 are surrounded (left and right) by identical imputed genotypes, then (ii) re-estimating error rates.

183 The filling procedure assumes that a double recombination event is very unlikely. The maximum region size  
 184 that is allowed for data filling can be calculated using the local recombination rate, which is calculated from  
 185 the data of the entire  $F_2$  population, imputed from Step 1. So, regions larger than the maximum size are left  
 186 unimputed. It is desirable to use an interference model to estimate the distances (in cM), for instance the one  
 187 implemented in the Kosambi mapping function (Kosambi 1944). The method employed in NOISYmputer to  
 188 estimate recombination fractions in  $F_2$  populations is the standard Expectation-Maximization algorithm  
 189 (Dempster *et al.* 1977).

190 Let's take the example of two SNPs A and C that define the bounds of such a region. They are separated by the  
 191 genetic distance  $d$  (cM). The maximum probability of a double crossover can be calculated as follows. We first  
 192 search for the SNP B that is the closest to the middle point between A and C (in cM). Then, we calculate the  
 193 recombination fractions  $r_{AB}$  and  $r_{BC}$  from  $d_{AB}$  and  $d_{BC}$  using the inverse of the Kosambi mapping function

194 
$$r = \frac{1}{2} \tanh(2d/100)$$

195 Note that  $r \approx \frac{d}{100}$  when  $d < 15$  cM. In the case of highly saturated maps, this formula can be used in most  
 196 intervals.

197 Then the maximum probability of the missing data to be different to the surrounding genotype is

198 
$$r_{ABC} = r_{AB} r_{BC} + r_{AB}^2 r_{BC}^2 \approx r_{AB} r_{BC} \text{ if SNPs A and C are homozygous}$$

199 
$$r_{ABC} = 2 r_{AB} r_{BC} + r_{AB}^2 r_{BC}^2 \approx 2 r_{AB} r_{BC} \text{ if SNPs A and C are heterozygous}$$

200 The regions for which  $r_{ABC} \leq \alpha$  are filled with the surrounding genotype;  $\alpha$  is set to 0.001 by default.

201 This step leaves the breakpoint regions unimputed.

202 We can then estimate new values for  $e_A$  and  $e_B$  by comparing the observed data with the newly imputed  
 203 regions. This is done by simply counting the proportion of A reads in BB-imputed segments, and the  
 204 proportion of B reads in AA-imputed segments.

### 205 Imputation - Step 3: Locating recombination breakpoints

206 Step 3 consists in imputing the SNP genotypes in the regions near the recombination breakpoints - i.e.,  
 207 between diplotypes of different states. The general idea is to determine an interval of high probability of  
 208 presence (loose support interval) of the breakpoint, then to calculate the likelihood of the data under the  
 209 hypothesis of a recombined segment.

210 This procedure allows determining with high confidence a loose support interval where the recombination  
 211 breakpoint is located. Here we take the example of a segment BB to the left of the breakpoint and a segment  
 212 AB to the right. Since we already know from Step 1 which are the two genotypes at the left and the right of the  
 213 breakpoint, we only need to consider the only two possible diplotypes, BB and AB. This saves one degree of  
 214 freedom.

215 If  $k$  defines the closest SNP position to the point where  $p(W_j = BB) = p(W_j = AB)$  in Step 1, we take  $k - 2m$   
 216 and  $k + 2m$  as starting points to guarantee that the breakpoint is covered by the interval. Then, for each  $SNP_j$   
 217 of the scanned area, we recalculate  $p(W_j = BB)$  and  $p(W_j = AB)$ , but this time in asymmetric windows of size  
 218  $m$ , that is, for BB, we define a window from  $SNP_j$  to  $SNP_j + m$  and for AB a window from  $SNP_j - m$  to  $SNP_j$ .  
 219 And then, following calculations similar to Step 1 but omitting the probabilities for the AA genotype:

220 
$$p(W_j = BB) = \exp(\rho_{BB}) / (\exp(\rho_{BB}) + \exp(\rho_{AB}))$$
 in the B window

221 
$$p(W_j = AB) = \exp(\rho_{AB}) / (\exp(\rho_{BB}) + \exp(\rho_{AB}))$$
 in the H window

222 Starting from  $k - 2m$ , and progressing to the right, we look for the first site  $SNP_j$  for which :

223 
$$P_{SI} = (1 - p(W_j = BB))(1 - p(W_j = AB)) > \alpha_{SI}$$
, with  $\alpha_{SI} = 0.05$  by default.

224 The breakpoint loose support interval is defined between the first position from the left ( $k_L$ ) and from right  
 225 ( $k_R$ ) where  $P_{SI} > \alpha_{SI}$ .

226 The breakpoint support interval and position are then estimated within the loose support interval. To do so,  
 227 for each  $SNP_j$  in the breakpoint interval  $k_L$  to  $k_R$ , a probability  $P_{bcp}$  that the diplotype's window contains a  
 228 breakpoint in its middle is estimated. We define a left window for  $p_{bcp}(W_j = BB)$  that includes the  $SNP_j$  and  
 229 goes to the left until the window's data count reaches  $m/2$  SNPs with at least one read (the left boundary of  
 230 this window is called  $m_L$ ) and a right window for  $p_{bcp}(W_j = AB)$  that starts at  $SNP_j + 1$  and goes to the right  
 231 until the window's data count reaches  $m/2$  SNPs with at least one read (the right boundary of this window is  
 232 called  $m_R$ ). Values of  $m_L$  and  $m_R$  are recalculated for each  $SNP_j$ .

233 The log-probabilities for the left and right segments are:

234 
$$\rho_{bcp}(W_j = BB) = \sum_{i=m_L}^j \log[p(G_i = BB)]$$

235 
$$\rho_{bcp}(W_j = AB) = \sum_{i=j+1}^{m_R} \log[p(G_i = AB)]$$

236 Then, the probability that the  $SNP_j$  and  $SNP_{j+1}$  are surrounding the breakpoint is:

237 
$$p_{bcp}(BK_j) = \exp(\rho_{bcp}(W_j = BB) + \rho_{bcp}(W_j = AB))$$

238 And after normalization:

239 
$$P_{bcp}(BK_j) = p_{bcp}(BK_j) / \max(p_{bcp}(BK_z): z = k_L, \dots, k_R)$$

240 The breakpoint is estimated in the middle of the interval defined by the SNP having the maximal  $P_{bcp}(BK_j)$   
 241 and the next SNP to its right.

242 Finally, the unimputed genotypes in the breakpoint area are completed in assigning the BB genotype to the  
 243 SNPs to the left of the SNP with the max  $P_{bcp}(BK_j)$  (included) and AB to the right.

244 Imputation of breakpoint positions for the other types of homozygous-heterozygous transitions (AB→BB,  
245 AA→AB, AB→AA) are easily derived from the example beforehand.

246 The support interval for the breakpoint around its most likely position can be defined in searching for the  
247 SNPs (left and right starting from the SNP with the maximum  $P_{b_{kp}}(BK_j)$ ) for which  $-\log_{10}(P_{b_{kp}}(BK_j)) \geq \alpha_{drop}$   
248 , where  $\alpha_{drop}$  is the dropping value of  $P_{b_{kp}}$ .  $\alpha_{drop}$  is set to 1 by default, corresponding to ten-fold decrease of  
249  $P_{b_{kp}}$  compared with  $P_{b_{kp}}(BK_j)$ .

## 250 Filtering options – before imputation

### 251 Genotypic frequencies, heterozygosity, missing data

252 The program can filter out SNPs for parental genotypes, and progeny heterozygosity, percentage of missing  
253 data and parental genotypic frequencies. Min and max filtering values can be manually entered (though  
254 usually not recommended), or the program can calculate them from the genotype matrix imported from the  
255 VCF. In this case, genotypic frequencies are calculated for each SNP, and the filter values are derived from the  
256 extreme percentiles of the frequency distribution. Correction factors can be applied to the percentiles, to avoid  
257 too small or too large values.

### 258 Read counts

259 SNPs with too few or too many reads can be eliminated. This can be useful to, for instance, remove SNPs in  
260 duplicated regions.

### 261 Incoherent SNPs

262 In sequence-based genetic mapping, it is common to observe SNPs that do not segregate the same way as their  
263 immediate environment, indicating a probable mapping error due to, for instance, structural variation  
264 between the reference genome and the population parents, or between the parents, or both. As segregation  
265 distortion is a frequent phenomenon in many organisms, the Mendelian expected frequencies cannot be used  
266 to analyze the SNP segregation. Instead, the procedure defines a window of  $n$  SNPs around each tested locus.  
267 By default,  $n=1\%$  the number of SNPs in the largest chromosome. For each window/SNP couple, it calculates  
268 the genotypes AA, BB and AB frequencies and the reads A and B frequencies across the population from the  
269 genotypes called in the VCF and compares the SNP with the window segregation of genotypes and reads using  
270 a chi-square test, where expected counts are the observed frequencies in the window multiplied by the  
271 population size. It then filters out SNPs for which the chi-square statistic exceeds a defined threshold for  
272 genotypes or reads frequencies.

## 273 Filtering options – after imputation

### 274 Incoherent chromosome segments (single individual)

275 Even after imputation and the different filtering operations, some few, improbable chromosome short  
276 diplotypes can still remain in the imputed matrix – we call them “small chunks”. The procedure identifies each  
277 small chunk composed of identical alleles, embedded in a homogeneous genomic environment that has a  
278 different allele. The method resembles the one used in Imputation - Step2.

279 Consider two SNPs A and C that define the bounds of a region imputed as H and surrounded by regions  
280 imputed as A or B. Search for the SNP B that is the closest to the middle point between A and C (in cM). Also  
281 search for an SNP D before the SNP A so that  $d_{DA} \sim d_{AB}$ , and an SNP E after the SNP C so that  $d_{CE} \sim d_{BC}$ .

282 Then, calculate the recombination fractions  $r_{DB}$  and  $r_{BE}$  from  $d_{DB}$  and  $d_{BE}$  using the inverse of the Kosambi  
283 mapping function. Then the maximum probability of the “chunk” to be different to the surrounding genotype  
284 is



285

$$r_{ABC} = r_{DB} r_{BE}$$

286 The chunks for which  $r_{ABC} \leq \alpha$  are restored with the surrounding genotype;  $\alpha$  is set to 0.001 by default.

## 287 Incoherent chromosome segments (cross-population)

288 Entire chromosome segments can be misplaced due to different kinds of genomic structural variation such as  
289 translocation, or duplication in one of the two parents that is not present in the reference genome. Such  
290 segments are called “aliens” in the program. If their size is too large, the chi-square procedure that filters out  
291 the incoherent SNPs may fail to identify them since it is run *before* the imputation. Alien segments are easily  
292 detected, as they produce severe map expansion. The procedure searches for SNPs that mark rapid changes in  
293 the slope of the cumulated centimorgans of the genetic map calculated from the imputed matrix. If a SNP  
294 marker is detected, the procedure then searches for the next SNP that is closely linked (by default  $r < 0.01$ ) to  
295 the SNP located just before the slope change. It then eliminates all the SNPs that are in-between.

## 296 Running the program

### 297 Algorithm implementation

298 The program is implemented in Java, as a Spring Boot (v2.6.7) project. Spring Boot is an open-source Java  
299 framework used to create standalone java applications. The executable .jar has been built with JDK 8 using  
300 Maven (v3.9.6), an open-source build tool.

301 Paths to datafiles and working folders paths, as well as parameters for imputation and filtering can be entered  
302 in a config file or directly in the command line. A “NOISYmputerResults” folder is automatically created, where  
303 the program writes all the output files.

### 304 Data specifications

305 In this current version, NOISYmputer is built and extensively tested to perform on  $F_2$  intercross data, that is,  
306 the progeny from  $F_1$  self-fertilization ( $F_2$ ). NOISYmputer can also be used on recombinant inbred lines by  
307 single seed descent from the  $F_2$  (SSD).

308 Input data for NOISYmputer are standard Variant Call Format (VCF) files, with chromosome coordinates.  
309 Genotypes (GT field) and allele depths (AD field) must be present in the VCFs. The data should be low  
310 coverage, that is, the sum of all sequences produced per sample is equivalent to 1-3 times (1-3 X) the size of  
311 the reference genome used. Ideally, the VCF should contain only bi-allelic single-nucleotide polymorphisms  
312 (SNPs), however NOISYmputer automatically filters out the other types of sites. Small indels are not handled.  
313 Parental lines need to be included in the VCF file with the prefix “Parent” in their name. Compressed “.gz” VCFs  
314 are accepted.

## 315 Results

316 NOISYmputer, FSFHap and LB-Impute were run on the IFB Core cluster (specs. available at  
317 <https://ifb-elixirfr.gitlab.io/cluster/doc/cluster-desc/>) with one allocated node per job and 32GB to 64GB of  
318 RAM to make sure that the tested programs are fully efficient.

319 Details on parameters used for the three imputation methods are provided in Supplementary Data 1.

### 320 Using simulations for calibration

321 To test NOISYmputer’s accuracy and precision in breakpoints estimation, we used simulated  $F_2$  datasets  
322 generated using PopSimul ([https://forge.ird.fr/diade/recombination\\_landscape/popsimul](https://forge.ird.fr/diade/recombination_landscape/popsimul)). A set of 84 VCFs  
323 with  $n = 300$  samples and varying values of marker density, mean depth and error rate were generated for a  
324 final expected map size of 180 cM (corresponding to an average of 3.6 breakpoints per sample) to mimic the  
325 chromosome 1 of rice. Using five different imputation window sizes, we compared the outputs of  
326 NOISYmputer to the known positions of breakpoints in the simulated data. In total, a set of 420 combinations

327 **Table 1.** Parameter values used in PopSimul to generate simulated  $F_2$  VCFs: marker density, mean depth and error rate. All  
328 possible combinations of these parameters were tested and imputed using a range of imputation windows in NOISYmputer.

Parameters	Marker density (in number of markers along the chromosome)	Mean depth (in X)	Error rate	NOISYmputer impute half window size	
Tested values	220,000	0.5	0.05	15	
	180,000	1	0.01	20	
	100,000	1.5	0.005	30	
	66,000	2			50
		2.5			100
		3			
		4			

329

330 were analyzed. All combinations and tested parameters are listed in Table 1. The results of these analyses  
331 confirmed that NOISYmputer efficiently detects the recombination breakpoints and precisely estimates their  
332 positions.

### 333 Breakpoint detection power

334 We assessed NOISYmputer's ability to correctly detect all breakpoints within samples by comparing positions  
335 of breakpoints found by NOISYmputer to those of simulated datasets. We considered a breakpoint correct  
336 when the simulated breakpoint position falls within NOISYmputer's loose support interval, along with the  
337 correct transition type.

338 Across all 420 VCFs, representing an average of 455,000 breakpoints, NOISYmputer demonstrated robust  
339 detection power, correctly finding 99.5% of simulated breakpoints (median at 99.6%). NOISYmputer also  
340 displayed high accuracy as, on average, 98.9% of breakpoints identified correspond to actual breakpoints  
341 (with a median at 100%). Thus, NOISYmputer presents an overall excellent accuracy and power in detecting  
342 breakpoints.

343 To better understand the impact of each parameter and their interaction on NOISYmputer performance, we  
344 performed a principal component analysis (PCA) on parameters and performance indicators. Accuracy was  
345 primarily influenced by error rates, but was also affected by the imputation window size when excessively  
346 large. Conversely, smaller window sizes enhanced detection power. Also, higher marker density correlated  
347 with improved detection power; as lower densities limit NOISYmputer's ability to identify breakpoints in  
348 regions with high recombination rates.

349 Some specific combinations decreased NOISYmputer detection accuracy and/or power but overall the lower  
350 performances were still acceptable. For instance, the lowest accuracy was of 72.3% (with error rates at 0.05  
351 and smaller imputation window size of 15), and the lowest power was of 96.9% (with larger imputation  
352 window size of 100). This is expected as small windows with high levels of noise are prone to false positive  
353 breakpoints. On the other hand, large windows (especially if coupled with low depth or marker density) may  
354 miss double recombination events, leading to false negatives (Figure 2 A and C). In more realistic conditions,  
355 error rates as high as 0.05 are not typically observed in Illumina sequencing and alignments. When removing  
356 runs with the 0.05 error rate, the average breakpoint accuracy reached 99.9%, with a median of 100%.  
357 Similarly, the average detection power was 99.6%, with a median of 99.5% (Figure 2B).

358 The data in the VCF files, such as sequencing depth or marker density or species model, depend on the model  
359 species or sequencing type and are generally not under the user's control. We thus looked for the imputation  
360 window size producing the best results for both breakpoint detection accuracy and power with the VCF that  
361 mimicked best the real  $F_2$  rice data we had. In both cases, the optimal results were obtained by the imputation  
362 half window size of 30. Thus, we used this value of 30 later on when exposing NOISYmputer to real datasets.

363

### 364 Precision of breakpoint position

365 NOISYmputer's precision was estimated by computing the difference between the simulated breakpoints  
 366 positions and the estimated ones by NOISYmputer. We considered the size of the support interval and its  
 367 marker density to estimate discrepancy (in number of SNPs) with the actual breakpoint position.

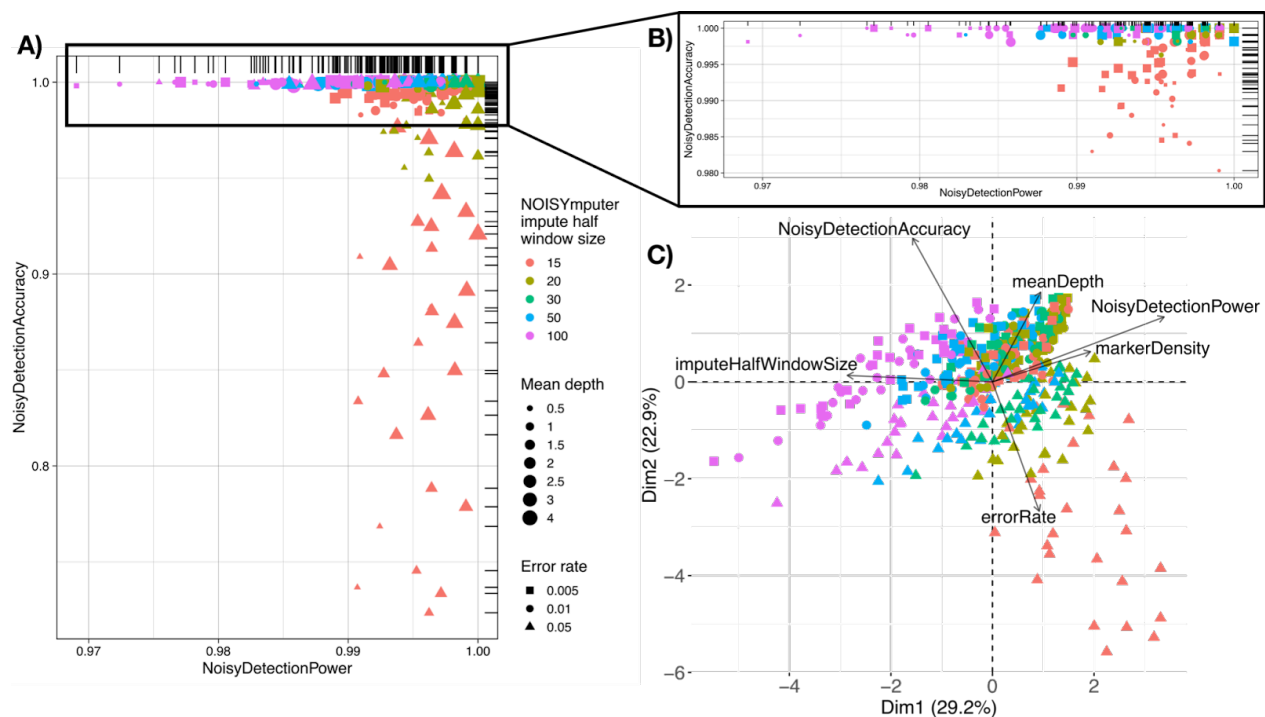
368 Across all 420 VCFs, a difference of 1,427 bp on average (equivalent to a discrepancy of  $\sim 2$  SNPs) was  
 369 observed. The median difference was even lower, with only 245 bp ( $< 1$  SNP discrepancy). This disparity  
 370 between the median and mean is mainly due to extreme combinations, particularly low depth combined with  
 371 high error rate. Notably, variance is higher in 0.5X coverage VCFs, becoming more homogeneous at 1X  
 372 coverage.

373 Regarding the imputation window, smaller half-windows resulted in lower average differences between  
 374 NOISYmputer and simulated positions but increased the median difference. Consequently, smaller windows  
 375 enhanced overall precision while potentially increasing the occurrence of extreme discrepancies.

### 376 Error rate estimations

377 Error rates ( $e_A$  and  $e_B$ ), are recalculated after a first iteration of imputation step 1. NOISYmputer correctly  
 378 estimated the error rates in 100% of the cases, with an average difference between simulated and estimated  
 379 error rates of  $9.8 \cdot 10^{-7}$  (standard deviation  $4.8 \cdot 10^{-5}$ ) (Supplementary Table S1). This reflects the accuracy of the  
 380 imputation, even with starting values for error rates far from the true values.

381



382

383 **Figure 2.** Most impacting parameters and data characteristics on NOISYmputer results based on 420 simulated  $F_2$  populations. **A)**  
 384 Representation of NOISYmputer's detection accuracy (proportion of NOISYmputer breakpoints being actual breakpoints from  
 385 simulated data) in function of NOISYmputer's detection power (proportion of simulated breakpoints correctly found by  
 386 NOISYmputer). NOISYmputer shows excellent power detection and accuracy with at least 72.3% and 96.9% respectively. **B)** Zoom  
 387 on the upper part of the A plot of detection accuracy and power, ignoring the error rate of 0.05. **C)** PCA Biplot of NOISYmputer  
 388 showing VCFs characteristics and imputation window size influencing detection accuracy and precision with simulated VCFs. The  
 389 lowest detection powers are observed when high error rates are coupled with a small imputation half-window size in  
 390 NOISYmputer. The lowest accuracies correspond to VCFs imputed with a large imputation half-window size in NOISYmputer and  
 391 can be accentuated by very low depth ( $\leq 1X$ ) and/or low marker density ( $< 66,000$  sites / 44 Mb).

## 392 Confirmed efficiency on real data and comparison with other methods

393 We assessed the performance of NOISYmputer on two real datasets: i) a maize F<sub>2</sub> population in GBS with 91  
394 samples, including the parents, and ii) a rice F<sub>2</sub> population with 3X coverage in whole-genome sequencing  
395 (WGS) comprising 222 samples, including the parents sequenced at ~30X. Details of how the real dataset for  
396 rice was generated are summarized in the Supplementary Data. The maize dataset is described in the  
397 LB-Impute publication (Fragoso *et al.* 2016).

398 In real data, direct estimation of imputation accuracy may be challenging due to the unknown true state at  
399 each locus. However, it is possible to assess the quality of the imputation indirectly by comparing the final  
400 genetic map to, for instance, existing high-quality maps. A correctly imputed dataset should yield a map size –  
401 in centimorgans (cM) – consistent with those derived from high-quality marker data. Conversely, datasets with  
402 a high rate of genotyping errors will exhibit map expansion, resulting in a longer genetic map due to falsely  
403 imputed recombination breakpoints.

404 Using map size estimates in centimorgans (cM) of chromosome 1 of these datasets, we compared the results of  
405 NOISYmputer to those of LB-Impute and FSFhap (Figure 3 and Table 2). Concerning the maize GBS dataset,  
406 LB-Impute and FSFhap strongly overestimated the map size expected from high-quality datasets (respectively  
407 633 cM and 13,271 cM), whereas NOISYmputer's map was in range with the expected map size (203 cM).  
408 Regarding the Rice WGS dataset, while both LB-Impute and FSFhap yielded maps much larger than expected  
409 (23,436 cM and 337,750 cM respectively), NOISYmputer estimated a map size close to the expected value (213  
410 cM). Also, results from FSFhap on PopSimul data produced very large map size estimations for high error rates  
411 (5%) VCF, while they were qualitatively similar to NOISYmputer's for lower (1% and .5%) error rates.

412 To further estimate the performance of NOISYmputer on real datasets we also performed comparisons on  
413 breakpoint detection accuracy, detection power, and position estimate in the 222 F<sub>2</sub> Rice population. This  
414 dataset includes 20 samples sequenced at ~20X depth, and artificially subsetted to 3X (that we call  
415 pseudo-3X). These 20 samples allow for a more robust evaluation as their breakpoints are well estimated  
416 thanks to their better depth. We processed similarly to the simulated analyses and compared breakpoint  
417 detection accuracy, power, and precision of breakpoint estimates for NOISYmputer against the accurately  
418 estimated breakpoints at 20X coverage. Unfortunately, we were not able to compare NOISYmputer results to  
419 those of FSFhap and LB-impute as, even if we managed to retrieve each breakpoint position estimate, we  
420 could not easily check which were actual breakpoints and which were false positives, as TASSEL FSFhap and  
421 LB-impute do not provide support intervals for breakpoints.

422 Overall, NOISYmputer demonstrated excellent results with, on average, 99% accuracy and 97% detection  
423 power. Regarding precision, on average the difference in position was of 10,219 bp, while the median was of  
424 only 415 bp. The large difference between the average and the median is due to a few breakpoints estimated  
425 far from their true position. Indeed, 80% of the breakpoints were still estimated at less than 1,669 bp from  
426 their true position. In terms of number of SNPs, the discrepancy was of 2 SNPs on average (median: 1)  
427 (Supplementary Table S2).

428 Overestimation of map sizes was mostly due to misinterpretation of noisy data by FSFhap and LB-Impute.  
429 These discrepancies frequently arise in regions corresponding to structural variations between parental  
430 genomes. Such variations can occur, for instance, when attempting to map onto regions found exclusively in  
431 the Parent A genome, which serves as the reference. In such cases, reads from B regions might map to the most  
432 similar A regions available resulting in false recombination events according to imputation softwares. This  
433 phenomenon is accentuated in WGS data compared to GBS data as the complete genome is sequenced and  
434 mapped, thus increasing the number of markers. Including more sites, inducing sites belonging to peculiar  
435 genomic structures, can hinder the quality of imputation if the software does not take into account the  
436 coherence of a marker with its surrounding environment in the population. Though FSFhap and LB-impute  
437 might be precise in the estimated breakpoints positions, their lack of accuracy in breakpoints detection leads  
438 to results, on whole genome datasets, difficult to use without the help of complex filtering steps. NOISYmputer,  
439 on the contrary, is very efficient at correcting mapping issues or divergence between parental genome  
440 structures.

441

442 **Table 2.** Comparison of estimated and expected map sizes for three different datasets using NOISYmputer, FSFHap and  
 443 LB-Impute. The 84 VCFs generated using PopSimul have varying numbers of markers (66,000, 100,000, 180,000 or 220,000),  
 444 depending on the settings used to generate the VCFs. Overall, NOISYmputer is showing considerably higher accuracy in map size  
 445 estimation compared to FSFHap and LB-Impute.

Dataset	Software	Estimated map size (cM)	Expected map size (cM)	Initial number of markers in VCF
<b>F<sub>2</sub> Maize GBS</b> <i>n</i> = 91 samples including parents	NOISYmputer	203		
	FSFHap	13,271	~200	17,945
	LB-Impute	633		
<b>F<sub>2</sub> Rice WGS</b> <i>n</i> = 222 samples including 30X parents	NOISYmputer	213		
	FSFHap	337,750	183	254,095
	LB-Impute	23,436		
<b>84 PopSimul F<sub>2</sub>s</b> <i>n</i> = 300 samples each including parents	NOISYmputer	180		
	FSFHap	479,399	180	Different number of markers depending on the simulation settings
	LB-Impute	N/A		

446

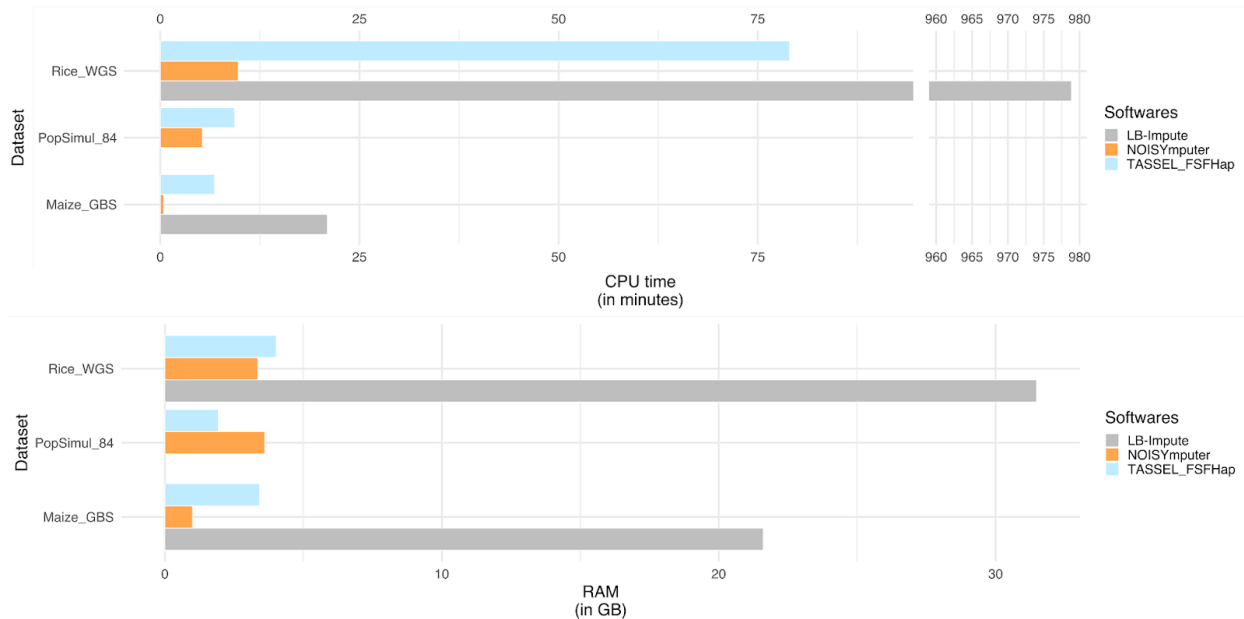
#### 447 A resource-optimized software, CPU- and RAM-efficient

448 In our comparative analysis of the NOISYmputer with established counterparts, we conducted comprehensive  
 449 benchmarks, focusing on execution time and RAM usage (Table 3 and Figure 3). To do so, we ran NOISYmputer,  
 450 FSFHap and LB-Impute on simulated and real datasets. We then retrieved their CPU time, “wall clock”  
 451 execution time and RAM usage using the *seff* command on the IFB computing cluster.

452 Concerning the F<sub>2</sub> Maize GBS dataset, NOISYmputer ran ~10 and ~45 times faster than FSFHap and LB-Impute,  
 453 respectively. It also used less RAM (~3.4 GB), ~3 times less than FSFHap and ~21 times less than LB-Impute.

454 Regarding the F<sub>2</sub> Rice WGS dataset, NOISYmputer used slightly less RAM than FSFHap and was ~13 times  
 455 faster (< 6 min vs. 1h19m). LB-Impute showed poor CPU and RAM efficiency as NOISYmputer used ~9 times  
 456 less RAM and ran ~145 times faster.

457 Due to the excessive computation time on this single smaller dataset, LB-Impute was excluded from the  
 458 remaining comparisons with the 84 PopSimul VCFs with 300 samples. It is interesting to note that FSFHap  
 459 resource efficiency is better on simulated than on real datasets even though they have more samples. Indeed,  
 460 FSFHap used on average 1.93 GB of RAM, whereas NOISYmputer was stable at 3.61 GB. NOISYmputer was still  
 461 faster than FSFHap on average, with ~5 min, while FSFHap ran in ~9 min. This underlies the difficulty that  
 462 FSFHap has to impute noisy data, partly due to structural variants and calling errors. These results underscore  
 463 NOISYmputer’s efficiency improvement in processing imputation tasks, especially compared to existing  
 464 software for bi-parental population imputation.



465

466 **Figure 3.** Barplot of CPU time and RAM resource usage for NOISYmputer (orange), LB-Impute (gray) and FSFHap (blue) on three  
467 datasets. Rice\_WGS is an  $F_2$  Rice WGS dataset with  $n = 222$  samples including parents; PopSimul\_84 values are averages across  
468 84 VCFs generated with PopSimul, each VCF containing  $n = 300$  samples including parents, simulated using ranges of depth,  
469 marker density and error rate to mimic different characteristics of  $F_2$  VCFs; Maize\_GBS is an  $F_2$  Maize GBS dataset with  $n = 91$   
470 samples including parents (with a lower marker density than Rice\_WGS). NOISYmputer is overly faster and more RAM-efficient in  
471 all conditions than FSFHap and LB-Impute, with the exception for RAM usage on simulated VCF files of PopSimul. No data is  
472 shown for PopSimul\_84/LB-Impute, as LB-Impute was not benchmarked due to excessive CPU time.

## 473 Availability and Future Directions

### 474 Availability

475 NOISYmputer is available as a multiplatform (Linux, macOS, Windows) Java executable at the URL  
476 [https://gitlab.cirad.fr/noisymputer/noisymputerstandalone/-/tree/1.0.0-RELEASE?ref\\_type=tags](https://gitlab.cirad.fr/noisymputer/noisymputerstandalone/-/tree/1.0.0-RELEASE?ref_type=tags). The  
477 source code and the documentation are available at the same URL. A Quarto markdown companion  
478 (compatible with R markdown and Jupyter notebooks IDE) that allows to display graphics of statistics (e.g.,  
479 genotypic frequencies on SNPs and samples) and graphical genotypes from NOISYmputer output files was  
480 developed and is also available.

481 NOISYmputer and its companion are distributed under the GNU Affero General Public License V3.0.

### 482 Future directions

#### 483 NOISYmputer's strengths

484 Although previous methods have made significant advances in addressing the challenges listed above, the  
485 noisiness of imputed datasets are still producing expanded genetic maps, excess heterozygosity, and  
486 probabilistically unlikely recombination events contained within a short physical interval. Here, we introduce  
487 an algorithm which, in a series of steps, addresses each source of error to create higher-quality datasets for  
488 improved trait mapping and genomics-assisted breeding. Our algorithm represents a step to systematically  
489 address all sources of NGS genotyping error and even errors in the reference genome, and hopefully the  
490 corrections brought here will be integrated into future algorithm development. Indeed, key features of  
491 NOISYmputer are its pre- and post-filtering steps that other currently available software does not perform. In  
492 filtering SNPs and segments that are incoherent with their environment and with the population local  
493 recombination landscape, NOISYmputer efficiently eliminates errors of genotype calling, sequencing errors, or  
494 errors generated by structural variants. The pre-imputation and post-imputation stages of NOISYmputer, in

495 **Table 3.** CPU and RAM usage of NOISYmputer, FSFHap and LB-Impute for three datasets based on the output of the *seff*  
 496 command on the IFB cluster. NOISYmputer 1st and 2nd Runs are displayed as NOISYmputer shows better CPU time usage for the  
 497 second run since the conversion of the raw VCF file has already been done. For LB-Impute, as imputation is processed in two  
 498 steps, CPU time and execution time results are the sum of the two steps; RAM usage corresponds to the highest RAM usage of  
 499 the two steps (offspring imputation). For the 84 PopSimul VCFs section, results correspond to the average of resource usage for  
 500 each of the 84 PopSimul VCFs for an imputation half-window of 30 SNPs with NOISYmputer and the default window size (50) of  
 501 FSFHap. All tests were conducted on the IFB Core cluster. \*As LB-impute showed excessive time and RAM consumption on the  
 502 Rice\_WGS dataset, we did not benchmark the 84 PopSimul VCFs with LB-impute.

Datasets	Software		CPU time (h:m:s)	Total execution time (h:m:s)	RAM (GB)
<b>F2 Maize GBS n = 91 samples including parents</b>	NOISYmputer	2nd Run	00:00:07	00:00:09	1.00
		1st Run	00:00:27	00:00:28	1.00
	FSFHap		00:06:49	00:04:35	3.42
	LB-Impute		00:20:59	00:21:04	21.61
<b>F2 Rice WGS n = 222 samples including 30X parents</b>	NOISYmputer	2nd Run	00:06:49	00:04:35	3.42
		1st Run	00:09:47	00:06:44	3.36
	FSFHap		01:19:00	01:19:06	4.02
	LB-Impute		16:18:52	16:19:21	31.48
<b>84 PopSimul VCFs with n = 300 samples each including parents</b>	NOISYmputer	1st Run	00:05:18	00:05:39	3.61
	FSFHap		00:09:20	00:09:24	1.93
	LB-Impute*		NA	NA	NA

503

504 particular, address artifacts of imputation caused by presence-absence variation misrepresented by the  
 505 reference assembly and assembly errors from inaccurate or misordered contigs. These imputation artifacts,  
 506 such as those caused by collapsed structural variants (incoherent sites or false heterozygosity) or  
 507 misassembled “chunks”, are not systematically addressed by other imputation methods, such as LB-Impute  
 508 (Fragoso *et al.* 2016), and otherwise must be parsed through manual filtering of the imputed dataset.

509 NOISYmputer is a resource-effective software developed in Java, allowing its integration in bioinformatics  
 510 pipelines. NOISYmputer is parallelizing computation at the sample level in several steps of the algorithm,  
 511 which increases its speed considerably. The use of a Java standalone executable also allows to simulate  
 512 parallelization in running each chromosome on a separate core of a server/cluster. Moreover, NOISYmputer  
 513 employs a maximum likelihood method, instead of hidden Markov models, which considerably reduces  
 514 computational complexity, compared to FSFHap (Swarts *et al.* 2014) and LB-impute (Fragoso *et al.* 2016),  
 515 while enhancing result accuracy and flexibility across diverse datasets. Indeed, NOISYmputer is less sensitive  
 516 to noisy regions (due to mapping artifacts for example) as it can handle large windows without being greedy  
 517 in RAM and computation time to overpass complex regions.

518 Notably, NOISYmputer's speed allows iterative refinement of parameter settings. For example, the size of the  
 519 imputation window (in number of SNPs), like in other imputation programs (e.g., FSFHap, LB-Impute), is  
 520 arbitrarily fixed by the user. The most appropriate value for *m* depends on several factors, including depth and  
 521 SNP density. A convenient way to determine which value for *m* to use is to run the imputation several times  
 522 with different values until reaching the expected distribution of the number of recombination breakpoints per  
 523 sample across the population (if previously known). Often, saturated genetic maps generated with other types  
 524 of markers are available in the literature, from which the expected distribution is easily derived. With our rice

525 data, the imputation algorithm gave the best results with  $m = 30$ , so even a few runs should provide a  
526 satisfying window size.

527 Furthermore, NOISYmputer generates a .json file from the VCF during the initial run, that is used by the  
528 consecutive runs, eliminating the redundant tasks of converting the input VCF file, thus enhancing speed for  
529 subsequent launches on the same dataset.

530 Its robust performance extends to various VCF characteristics, accommodating differences in SNP quality,  
531 marker density, error rates, and sequencing depths. This is partly due to its low sensitivity to the SNP calling  
532 step used to generate the input VCF, as NOISYmputer is re-estimating the probabilities of genotypes using the  
533 allele depth at each site, along with information of the surrounding environment and of the whole population.  
534 This results in maintenance of overall excellent detection accuracy, detection power and position precision on  
535 recombination breakpoints even with very low coverage datasets ( $\leq 1X$ ). However, users should exercise  
536 caution in selecting an appropriate imputation window size to mitigate the risk of false positives and  
537 negatives.

538 In addition to its performance benefits, NOISYmputer provides users with several comprehensive breakpoint  
539 confidence information allowing to further filter the identified breakpoints. This is a feature that is innovative  
540 and useful and not available in other software, to our knowledge. NOISYmputer also outputs statistics on  
541 genotypic/allelic frequencies, samples and genetic map among others.

## 542 Suggestions for Improvement

543 NOISYmputer could benefit from several improvements. The first one is including more population types. In  
544 the next version, we will implement  $F_2$  backcross, or  $BC_1F_1$ , the progeny of the  $F_1$  hybrid crossed with one of  
545 the parents ( $BC_1$ ) ; doubled haploid of  $F_1$  gametes (DH) ;  $F_2$  intercross, that is, the progeny from  $F_1$   
546 self-fertilization ( $F_2$ ); recombinant inbred lines by single seed descent from the the  $BC_1F_1$  (BCSSD); the  
547 unconventional mating design (UMD)  $BC_1F_3$ , derived by two generations of self-fertilization of  $BC_1F_1$   
548 individuals. For now, it has been extensively tested and optimized for  $F_2$  crosses between distant parents  
549 which might be one of the hardest designs to estimate breakpoints from. We thus are confident that the  
550 algorithm can be adapted to these other types of crosses.

551 Breakpoint detection and accuracy could benefit from a more complex modeling of the likelihood. Currently,  
552 we test for the existence of a single transition within the loose support interval in imputation Step 3. Testing  
553 for one, two or even three transitions in a single interval could increase the probability of finding close double  
554 recombination events if they happened to have a higher probability in the tested region. Breakpoint position  
555 estimation, on the other hand, might be improved by using a combination of NOISYmputer's current algorithm  
556 with a hidden markov model occurring in the Step 3 of imputation. This way, a smaller window size could be  
557 applied and the region to scan would be reduced to a very limited percentage of the genome only, resulting in a  
558 considerable gain of time.

559 NOISYmputer is robust on a broad range of samples and its computation time makes it very convenient. Part of  
560 the success of NOISYmputer lies in the fact that it performs pre- and post-imputation filtering steps that  
561 remove, among other things, incoherent SNPs, meaning SNPs that do not segregate the same way as its  
562 immediate environment, often indicating mapping errors. This filtering of incoherent SNPs step uses a  
563 Chi-square test to evaluate if the observed pattern is reasonable. Unfortunately, Chi-square test thresholds are  
564 dependent on sample sizes. Thus, when imputing many samples (e.g.,  $m=2000$ ) with NOISYmputer, the user  
565 has to adapt the Chi-square threshold to the sample size, which is not convenient. A solution to this would be  
566 to use a "Cramér's  $V$ " statistic instead (Cramér 1999), which would be independent of the sample number in  
567 the VCF.

568 Unlike FSFHap or LB-Impute, NOISYmputer does not impute the parental genotypes, which might result in the  
569 loss of SNPs, especially in datasets derived from very low-coverage sequencing. Although we recommend  
570 sequencing the parents at high coverage ( $> 20X$ ), it is not always possible – for instance, when re-analyzing  
571 historical data. The next version of NOISYmputer will impute the parental genotypes when necessary.

572 Finally, as pointed in the Results section, the imputation half-window size can have an impact on the outputs of  
573 NOISYmputer. NOISYmputer could benefit from an iterative process that would check for different window



574 sizes and analyze the convergence of the results to select the appropriate window size and thus to achieve the  
575 best compromise between detection accuracy and power, along with precision.

## 576 Acknowledgements

577 We thank Karine Labadie (CEA, Institut de Génomique, Genoscope, Evry, France) for sharing the WGS data for  
578 the sequencing of rice populations, Christine Tranchant-Dubreuil (IRD, Montpellier, France) for her help with  
579 retrieving the Rice\_WGS data and François Sabot (IRD, Montpellier, France) for coordinating the IRIGIN  
580 project. We are grateful to the Institut Français de Bioinformatique (IFB) for providing computing resources.  
581 We also thank the Yale Center for Research Computing for guidance and use of the research computing  
582 infrastructure. The following programs supported parts of this initiative: the French ANR project "LANDSREC"  
583 (ANR-21-CE20-0012-03), the French Government France Génomique program through its International Rice  
584 Genome INitiative "IRIGIN" project, and the CGIAR Research Program "RICE".

## 585 Author's contributions

586 CT participated to the algorithm development, designed and ran the bioinformatics pipeline to call SNPs for  
587 the WGS dataset ( $F_2$  and SSD), benchmarked and compared all softwares, wrote the quarto markdown  
588 companion, tested the program for debugging and took part in the manuscript conception. AB participated in  
589 the algorithm development and implemented it in Java, took part in the manuscript conception. CF helped  
590 with running LB-Impute for the Rice\_WGS dataset for the previous version of NOISYmputer and edited the  
591 manuscript. AG designed and ran the bioinformatics pipeline to call SNPs for the Rice\_WGS dataset for the  
592 previous version of NOISYmputer. JFR took part in the initial design and definition of specifications for  
593 NOISYmputer. ML conceptualized the initial imputation algorithm for NOISYmputer, participated in its further  
594 development and took part in the manuscript conception.

## 595 References

- 596 Browning S. R., and B. L. Browning, 2007 Rapid and Accurate Haplotype Phasing and Missing-Data Inference  
597 for Whole-Genome Association Studies By Use of Localized Haplotype Clustering. *The American*  
598 *Journal of Human Genetics* 81: 1084–1097. <https://doi.org/10.1086/521987>
- 599 Browning B. L., X. Tian, Y. Zhou, and S. R. Browning, 2021 Fast two-stage phasing of large-scale sequence data.  
600 *The American Journal of Human Genetics* 108: 1880–1890.  
601 <https://doi.org/10.1016/j.ajhg.2021.08.005>
- 602 Cramér H., 1999 *Mathematical Methods of Statistics*. Princeton University Press.
- 603 Davey J. W., and M. L. Blaxter, 2010 RADSeq: next-generation population genetics. *Briefings in Functional*  
604 *Genomics* 9: 416–423. <https://doi.org/10.1093/bfgp/elq031>
- 605 Dempster A. P., N. M. Laird, and D. B. Rubin, 1977 Maximum Likelihood from Incomplete Data via the EM  
606 Algorithm. *Journal of the Royal Statistical Society. Series B (Methodological)* 39: 1–38.
- 607 Elshire R. J., J. C. Glaubitz, Q. Sun, J. A. Poland, K. Kawamoto, *et al.*, 2011 A Robust, Simple  
608 Genotyping-by-Sequencing (GBS) Approach for High Diversity Species, (L. Orban, Ed.). *PLoS ONE* 6:  
609 e19379. <https://doi.org/10.1371/journal.pone.0019379>

- 610 Fragoso C. A., C. Heffelfinger, H. Zhao, and S. L. Dellaporta, 2016 Imputing Genotypes in Biallelic Populations  
611 from Low-Coverage Sequence Data. *Genetics* 202: 487–495.  
612 <https://doi.org/10.1534/genetics.115.182071>
- 613 Heffelfinger C., C. A. Fragoso, M. A. Moreno, J. D. Overton, J. P. Mottinger, *et al.*, 2014 Flexible and scalable  
614 genotyping-by-sequencing strategies for population studies. *BMC Genomics* 15: 979.  
615 <https://doi.org/10.1186/1471-2164-15-979>
- 616 Howie B., C. Fuchsberger, M. Stephens, J. Marchini, and G. R. Abecasis, 2012 Fast and accurate genotype  
617 imputation in genome-wide association studies through pre-phasing. *Nat Genet* 44: 955–959.  
618 <https://doi.org/10.1038/ng.2354>
- 619 Huang X., Q. Feng, Q. Qian, Q. Zhao, L. Wang, *et al.*, 2009 High-throughput genotyping by whole-genome  
620 resequencing. *Genome Res.* 19: 1068–1076. <https://doi.org/10.1101/gr.089516.108>
- 621 Kosambi D. D., 1944 The Estimation of Map Distances from Recombination Values, pp. 125–130 in *D.D.*  
622 *Kosambi: Selected Works in Mathematics and Statistics*, edited by Ramaswamy R. Springer India, New  
623 Delhi.
- 624 Swarts K., H. Li, J. A. Romero Navarro, D. An, M. C. Romay, *et al.*, 2014 Novel Methods to Optimize Genotypic  
625 Imputation for Low-Coverage, Next-Generation Sequence Data in Crop Plants. *The Plant Genome* 7:  
626 plantgenome2014.05.0023. <https://doi.org/10.3835/plantgenome2014.05.0023>
- 627 Xu C., Y. Ren, Y. Jian, Z. Guo, Y. Zhang, *et al.*, 2017 Development of a maize 55 K SNP array with improved  
628 genome coverage for molecular breeding. *Mol Breeding* 37: 20.  
629 <https://doi.org/10.1007/s11032-017-0622-z>
- 630

